Available online at www.sciencedirect.com
ScienceDirect
Journal of the European Ceramic Society 29 (2009) 3299–3306
www.elsevier.com/locate/jeurceramsoc

Sintering and crystallisation of 45S5 Bioglass® powder

Oana Bretcanu [a,1], Xanthippi Chatzistavrou [a], Konstantinos Paraskevopoulos [b], Reinhard Conradt [c], Ian Thompson [d], Aldo R. Boccaccini [a,*]

[a] *Department of Materials, Imperial College London, Prince Consort Rd., London SW7 2BP, UK*
[b] *Department of Physics, Aristotle University of Thessaloniki, Thessaloniki 54124, Greece*
[c] *Institut fuer Gesteinshuettenkunde, RWTH Aachen, 52056 Aachen, Germany*
[d] *Department of Biomaterials, King's College London Dental Institute, London SE1 9RT, UK*

Received 29 March 2009; received in revised form 14 June 2009; accepted 24 June 2009
Available online 24 July 2009

Abstract

The sintering process of 45S5 Bioglass® powder (mean particle size < 5 μm) was investigated by using different thermal analysis methods. Heating microscopy and conventional dilatometry techniques showed that bioactive glass sinters in two major steps: a short stage in the temperature range 500–600 °C and a longer stage in the range 850–1100 °C. The optimal sintering temperature and time were found to be 1050 °C and 140 min, respectively. Differential thermal analysis (DTA) showed that Bioglass® crystallises at temperatures between 600 and 750 °C. The characteristic crystalline phases were identified by Fourier Transformed Infrared Spectroscopy (FTIR), Transmission Electron Microscopy (TEM) and X-Ray Diffraction (XRD). The crystallisation kinetics was studied by DTA, using a non-isothermal method. The Kissinger plot for Bioglass® powder heated at different heating rates between 5 and 30 °C/min yielded an activation energy of 316 kJ/mol. The average value of Avrami parameter determined using the Augis–Bennett method was 0.95 ± 0.10, confirming a surface crystallisation mechanism. After sintering at 1050 °C for 140 min, the main crystalline phase was found to be $Na_2Ca_2Si_3O_9$. The results of this work are useful for the design of the sintering/crystallisation heat treatment of Bioglass® powder which is used for fabricating tissue engineering scaffolds with varying degree of bioactivity.

Keywords: A. Sintering; B. Microstructure-final; C. Thermal properties; E. Structural applications; Bioglass®

1. Introduction

45S5 Bioglass® is a commercially available inorganic material, which has been used as bone replacement for more than 20 years.[1] This is the first bioactive glass developed by Hench et al. in 1969 [2] and has the following chemical composition: 45 wt.% SiO_2, 24.5 wt.% Na_2O, 24.5 wt.% CaO and 6 wt.% P_2O_5. This glass is highly bioactive and it is both osteoinductive and osteoconductive, enabling its application in bone tissue engineering.[3,4] Moreover, it has been shown that the ionic dissolution products of 45S5 Bioglass® may enhance new bone formation (osteogenesis) through a direct control over genes that regulate cell induction and proliferation.[5]

45S5 Bioglass® has been used for fabrication of scaffolds for bone tissue engineering by sintering powders of particle size < 5 μm and employing the foam replication technique.[6] The success of the scaffold fabrication process depends on the sintering ability of the Bioglass® powder since this particular bioactive glass composition is prone to crystallisation at the high temperature required for sintering, as also investigated by several authors.[7–11] Therefore, the requisite for optimising the fabrication of Bioglass® scaffolds is to understand the sintering conditions of Bioglass® particles and the interaction between sintering and crystallisation of the material. By knowing the structural transformations which occur during the heat treatment of Bioglass®, the scaffold fabrication process can be tailored, e.g. in terms of achieving the highest possible density of the foam struts and the required crystallinity which itself controls the material bioactivity.[12]

Previous studies have shown that there are five structural transformations during the heating of Bioglass® up to 1000 °C: a first glass transition, a glass-in-glass phase separation, two

* Corresponding author. Tel.: +44 2075946731; fax: +44 2075946757.
E-mail address: a.boccaccini@imperial.ac.uk (A.R. Boccaccini).
[1] Current address: Materials Science and Chemical Engineering Department, Politecnico di Torino, Italy.

0955-2219/$ – see front matter © 2009 Elsevier Ltd. All rights reserved.
doi:10.1016/j.jeurceramsoc.2009.06.035

crystallisation processes and a second glass transition.[12–14] Modelling of the sintering behaviour of bioactive glass scaffolds has been also considered recently[15] but there is still a lack of knowledge about the effect of different process variables on the final microstructure of the partially crystallised Bioglass®.

The aim of this work was to study the sintering process of 45S5 Bioglass® powder by using different thermal analysis methods; including dilatometry, differential thermal analysis (DTA) and, for the first time, heating microscopy to investigate sintering anisotropy effects. The crystalline phase characterisation after the crystallisation and sintering process was carried out by Fourier Transformed Infrared Spectroscopy (FTIR), Transmission Electron Microscopy (TEM) and X-Ray Diffraction (XRD) techniques.

2. Experimental procedures

2.1. Materials

Bioglass® (type 45S5) powder (NovaMin USA) of mean particle size <5 μm was used in this investigation. The chemical composition was given in Section 1. This glass is being used for fabrication of tissue engineering scaffolds by the foam replica method,[6] as mentioned above.

2.2. Heating microscopy

The sintering process of Bioglass® powder compacts was directly observed by heating microscopy. This technique allows the quantification of sintering variables by measuring the variation of the sample dimensions during the heating process.[16] A Leitz-Wetzlar heating stage optical microscope was used and sintering was investigated in air atmosphere, using a heating rate of 20 °C/min. The samples were obtained by pressing manually the Bioglass® powder using a rectangular die. The nominal relative density of the fabricated samples ("green" density) was ~0.50. The specimens were observed by a video camera and images of the specimen silhouettes during sintering were registered up to 1150 °C. The shrinkage–temperature curves were analysed by using three different samples and the results were averaged. The samples' shrinkage was calculated at specific temperatures from the variation of the samples' area, using the following equation, which assumes isotropic shrinkage:

$$\text{shrinkage}(\%) = \frac{A_0 - A_T}{A_0} 100 \quad (1)$$

where A_0 = the initial area of the specimen at room temperature; A_T = the area of the specimen at temperature T.

The variation of sample shrinkage with time and temperature was registered by heating the samples up to 1050 °C using a heating rate of 20 °C/min. In addition, isothermal sintering was investigated by holding the green body samples at 1050 °C for 200 min in the heating microscope. Images of the sample silhouettes were taken every 5 min. The experiment was repeated three times, using three different samples and the results were averaged. The samples' shrinkage was calculated at each time point from the variation of the samples' area, using the following equation:

$$\text{shrinkage}(\%) = \frac{A_{t0} - A_t}{A_{t0}} 100 \quad (2)$$

where A_{t0} = the area of the specimen at time 0 at 1050 °C; A_t = the area of the specimen at time t at 1050 °C.

In a separate set of experiments to assess possible shrinkage anisotropy, heating microscopy was carried out on cylindrical specimens monitoring the axial (height) and radial shrinkage at temperatures of up to 1150 °C using three different heating rates: 3, 10 and 20 °C/min. The starting samples were of 2 mm diameter and 2 mm height and were obtained by pressing the Bioglass® powder in a cylindrical die. Three different specimens were used for each heating rate. During the sintering process, the specimens' silhouettes were recorded by a video camera. The height and diameter of the silhouettes were measured at different time points and the results were averaged. The axial and radial shrinkage were calculated using the following equations:

$$S_H = \frac{\Delta H}{H_0} = \frac{H_0 - H_i}{H_0} \quad (3)$$

$$S_D = \frac{\Delta D}{D_0} = \frac{D_0 - D_i}{D_0} \quad (4)$$

where S_H = axial shrinkage; H_0 = initial height of the samples at room temperature; H_i = height of the samples at time i; S_D = radial shrinkage; D_0 = initial diameter of the samples at room temperature; D_i = diameter of the samples at time i.

If the samples sinter isotropically, the axial and radial shrinkage are equal ($S_H = S_D$). On the contrary, for anisotropic sintering behaviour, $S_H \neq S_D$. By plotting the axial versus radial shrinkage, the isotropic/anisotropic characteristics of the specimens can be determined.[17] A more convenient way to quantify the shrinkage anisotropy of sintering materials is the calculation of the shrinkage anisotropy factor k. This parameter can be calculated with the following equation[17]:

$$k = \frac{S_D}{S_H} \quad (5)$$

If $k = 1$, the sintering is isotropic; if $k \neq 1$, the sintering is anisotropic. In the present study the evolution of k with sintering time was investigated.

2.3. Dilatometry

The sintering temperature of Bioglass® powder compacts was also determined using dilatometry measurements. Cylindrical pellets having 5 mm diameter and 8 mm length were obtained by uniaxial pressing. A Netzsch dilatometer 402 E was used to measure the shrinkage of the samples during heating up to 1150 °C with a heating rate of 10 °C/min. The relative variation of the sample's length ($\Delta L/L_0$) during heating was measured directly by the instrument where L_0 is the initial length of the cylindrical sample and ΔL is the variation of the sample's length at a given temperature.

2.4. Differential thermal analysis (DTA)

DTA of Bioglass® powder was performed on a PL Thermal Sciences STA 1500 DCI instrument. The measurements were carried out in air, up to 1250 °C, using a range of heating rates between 5 and 30 °C/min. Pure alumina powder was used both as reference material and for base line determination. The Bioglass® characteristic temperatures (glass transition temperature, crystallisation temperature and melting temperature) were determined directly from the DTA plots. The crystallisation kinetics was studied by DTA using a non-isothermal method. The activation energy for crystallisation (E) was calculated from the Kissinger equation[18]:

$$\ln\left(\frac{\alpha}{T_p^2}\right) = -\frac{E}{RT_p} + \text{constant} \quad (6)$$

where E = activation energy (kJ/mol); α = heating rate (K/min); T_p = peak crystallisation temperature; R = gas constant (8.32 J K^{-1} mol^{-1}).

By plotting $[-\ln(\alpha/T_p^2)]$ versus $1/T_p$ the activation energy of crystallisation can be calculated from the slope of the curve.

The mechanism of nucleation and growth of crystals can be defined by the Avrami parameter, n, which can be determined by the Augis–Bennet equation.[18]

$$n = \frac{2.5}{\Delta T}\frac{RT_p^2}{E} \quad (7)$$

where ΔT (K) is the width of the crystallisation peak at the half maximum. If $n \approx 1$, crystallisation occurs from the surface (surface crystallisation). If $n \approx 3$, crystallisation takes place from the volume (volumetric crystallisation).[19] When surface crystallisation is dominant ($n = 1$), the nuclei are formed prior to or during the thermal treatment.[20]

Another parameter used for evaluation of the glass crystallisation ability is the Hruby coefficient (Hr) given by Eq. (8):

$$Hr = \frac{T_p - T_g}{T_m - T_p} \quad (8)$$

where Hr = Hruby coefficient; T_p = peak crystallisation temperature; T_g = glass transition temperature; T_m = onset melting temperature (beginning of the melting process).

The higher the value of Hr, the lower is the crystallisation tendency of the material.[21]

2.5. FTIR

FTIR measurements were carried out by using a Bruker spectrometer IFS 113 V, the spectra were collected in the reflectance mode, in MIR region (5000–400 cm^{-1}) and for each spectrum 128 consecutive scans were recorded with a resolution of 2 cm^{-1}. Samples of Bioglass® powder were characterised before the heat treatment and at characteristic temperatures (570, 700 and 800 °C). The sample preparation was performed by obtaining a quantity of Bioglass® in powder form and pressing it in a vacuum press at 7 t, in order to produce pellets with diameter of 13 mm and thickness of 0.8 mm.

2.6. TEM

The TEM study was performed on samples of Bioglass® heat treated up to 800 °C, using a conventional TEM (JEM 100C) working at 100 kV. Appropriate specimens were prepared by mechanical polishing and ion beam thinning.

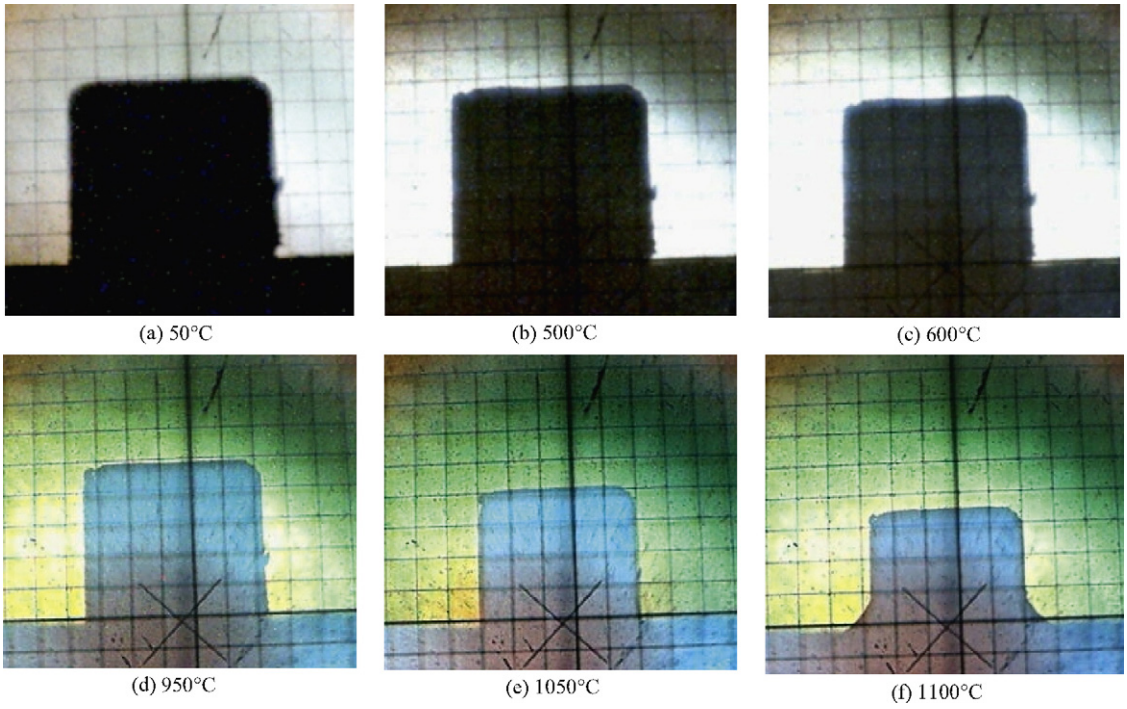

Fig. 1. Heating microscope silhouettes of a cubic Bioglass® sample at different characteristic temperatures during sintering up to 1100 °C with heating rate 20 °C/min.

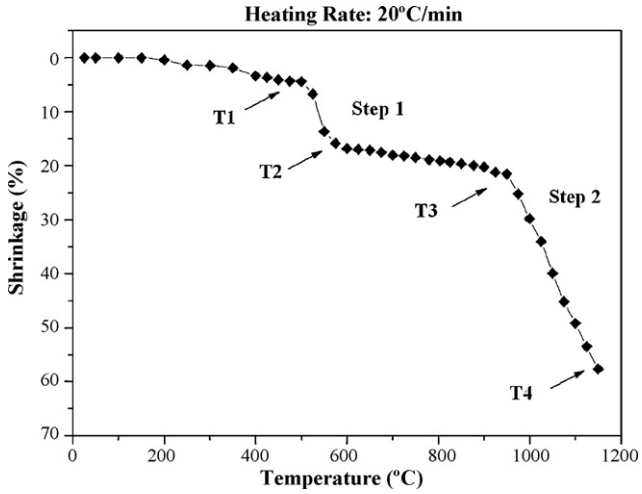

Fig. 2. Variation of shrinkage of Bioglass® powder compacts as function of temperature for a heating rate of 20 °C/min (cubic samples).

2.7. XRD

XRD measurements on Bioglass® powders before heat treatment, after crystallisation at 800 °C and after sintering at 1050 °C for 140 min were carried out using a Philips X'Pert diffractometer with Cu Kα radiation, using a step of 0.04° (2θ) and a time per step of 2 s. The diffraction lines were identified using "X'Pert HighScore" program, with PCPDFWIN database (2002 JCPDS-International Centre for Diffraction Data).

3. Results and discussion

3.1. Heating microscopy

Typical heating microscope silhouettes of cubic Bioglass® samples during sintering at a heating rate of 20 °C/min and at different characteristic temperatures are shown in Fig. 1. The reduction of the sample dimensions during the sintering process can be noticed. The dimensional changes of the sample can be clearly appreciated by comparing the two images at 50 and 1100 °C. The sample seems to keep the cubic shape up to 1100 °C (Fig. 1a–e). At 1100 °C the sample started to melt and the shape of the silhouette changes (Fig. 1f). Increasing the temperature further, the glass becomes softer and viscosity significantly decreases. Melting starts from the surface and the glass specimen deforms under its own weight, thus, the bottom part of the sample expands becoming more rounded, while the top of the sample starts to distort.

The variation of shrinkage as function of sintering temperature (Eq. (1)) is illustrated in Fig. 2. Two distinct sintering steps can be distinguished: a first stage (step 1) and a longer and more marked stage (step 2). The first densification step starts at 500 °C (T1) and ends at 600 °C (T2). The second densification step starts at 950 °C (T3). The shrinkage associated to the first step is around 12%. While samples were found to shrink more during the second densification step (around 36%). Between T2 and T3, the samples shrink about 5% and the plotted shrinkage curve indicates a horizontal plateau. All samples start to melt at around 1100 °C (T4). The four characteristic temperatures are indicated in Table 1. The sintering temperatures for the Bioglass® samples are included in the interval 1000–1100 °C when the higher densification is obtained. As can be seen in Fig. 1e, the sample still keeps its shape at 1050 °C, however possible anisotropic shrinkage effects are considered further below. The study of shrinkage versus time (Eq. (2)) was therefore carried out at 1050 °C. The obtained graphic is presented in Fig. 3. The optimum sintering time at 1050 °C can be considered to be 140 min, where the curve of shrinkage (%) versus time reaches a plateau. The isothermal sintering study confirms that additional shrinkage occurs (about 15%), resulting in a total shrinkage of about of 55%. Therefore under isothermal conditions Bioglass® powder compacts should be sintered at 1050 °C for 140 min to achieve maximal densification. This finding is very important in terms of understanding the structural transformations during sintering of Bioglass® powder leading to dense materials. The further fine tuning of these parameters will be required to develop the optimised fabrication process for porous scaffolds from the same Bioglass® powder. Indeed sintering at temperatures in the range 1000–1100 °C was used in previous studies to fabricate foam-like scaffolds with open porosity and highly dense struts.[6]

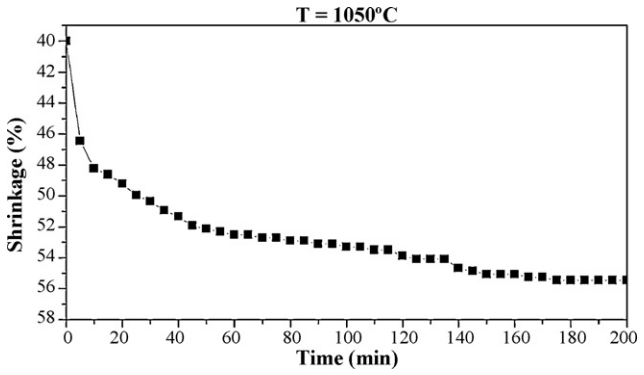

Fig. 3. Variation of shrinkage versus time during isothermal sintering of Bioglass® powder compacts at 1050 °C (cubic samples).

The variation of sample dimensions (height H and diameter D) of cylindrical samples during sintering at different heating rates is shown in Fig. 4. To put in evidence the rate of densification, shrinkage is plotted against sintering time for the three different sintering rates investigated (3, 10 and 20 °C/min). The shape of the curves is similar for both height and diameter and

Table 1
Sintering characteristic temperatures determined from the shrinkage–temperature curves by heating microscopy and dilatometry techniques.

Type analysis	T1 (°C)	T2 (°C)	T3 (°C)	T4 (°C)	T5 (°C)
Heating microscopy (rate 20 °C/min)	500	600	950	1100	–
Dilatometry (rate 10 °C/min)	530	620	850	1130	1050

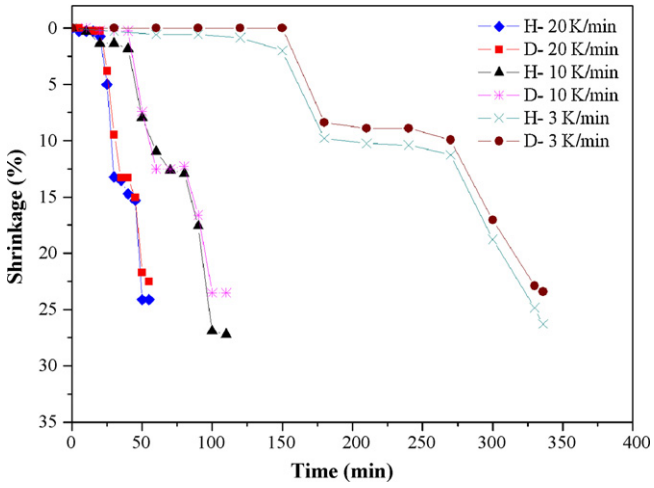

Fig. 4. Variations of the dimensional characteristics (height H and diameter D) of the cylindrical Bioglass® samples versus time at different heating rates: 3, 10 and 20 °C/min up to 1150 °C.

the two steps of sintering discussed above can be identified in all curves. It can be noticed that with increasing heating rate (from 3 to 20 °C/min), the shrinkage rates (given by the slopes of the curves in Fig. 4) decrease for both sintering stages. Moreover the length of the plateau (between T2 and T3) increases with decreasing heating rate. At a low heating rate, the particles are exposed longer time to high temperature, which tends to favour crystallisation over viscous flow densification, as discussed elsewhere.[17] It was also observed that the duration of the first step of shrinkage increases significantly with increasing heating rate. This result indicates that at higher heating rates a higher densification can be achieved during the first step, which is also ascribed to the competition between the viscous flow sintering and crystallisation phenomena.

Fig. 5 shows a plot of radial (diametral) shrinkage (Eq. (4)) versus axial shrinkage (Eq. (3)) during sintering of cylindrical samples at different heating rates in the heating microscope. As can be seen in this figure, most data are located close to the isotropic line, indicating that sintering of Bioglass® powder

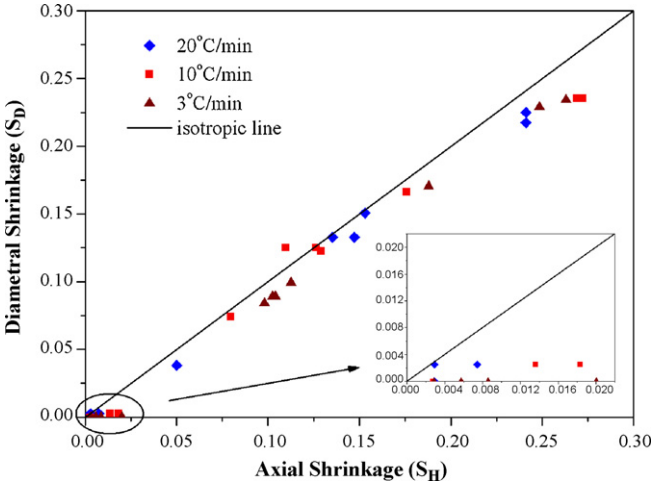

Fig. 5. Diametral shrinkage versus axial shrinkage during sintering of cylindrical samples in heating microscope.

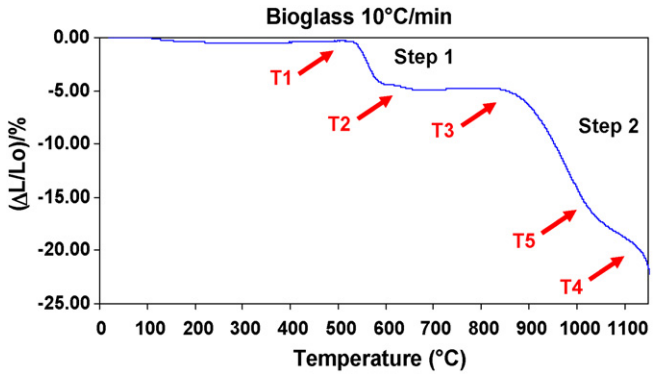

Fig. 6. Dilatometric curve of Bioglass® powder compacts obtained at a heating rate of 10 °C/min.

under the conditions investigated has only a slightly anisotropic character. However, in all cases the axial shrinkage is seen to be slightly higher than the diametral shrinkage indicating that the shrinkage anisotropy factor will be <1. The shrinkage is more anisotropic in the early stages of sintering and reaches values close to 1 (at $T > 850$ °C) with the progress of densification. For the heating rate of 3 °C/min the shrinkage anisotropy factor reaches a value $k = 0.87$ at 600 °C, remaining constant at higher temperatures. This result can be related to the increased crystallisation of this sample. For the heating rate of 20 °C/min the k factor increases to $k = 0.95$ at temperatures > 750 °C. These results indicate a complex shrinkage anisotropy dependence on heating rate, probably affected by crystallisation of the sample. In addition, the possible different coordination number of particles in different directions may have an effect, since the number of contacts between particles is expected to be higher along the specimen length in uniaxially pressed samples. Overall, however the anisotropy is negligible and it should not cause major distortion of the shape of structures made by sintering, including scaffolds.[6]

3.2. Dilatometry

The relative variation of the sample length ($\Delta L/L_0$) versus temperature during heating up to 1150 °C is plotted in Fig. 6 for a heating rate of 10 °C/min. The two major sintering steps are clearly visible. The first densification step is seen to start at 530 °C (T1) and to end at 620 °C (T2), while the second densification step starts at 850 °C (T3) and melting occurs at 1130 °C (T4). The first step shrinkage is around 5% and the second step shrinkage is around 16%. The plateau between T2 and T3 is quite horizontal (Fig. 6). The second sintering step presents a small inflexion at 1050 °C (T5), probably corresponding to a softening point when viscous flow starts. The characteristic sintering temperatures are summarised in Table 1. The results are similar to those obtained by heating microscopy (Fig. 2). The differences depend only on the instruments' different sensibility and on the heating rates used. By using a slower heating rate, the shape of the shrinkage–temperature curve becomes better defined. Also from dilatometry results, it is confirmed that the sintering temperature for Bioglass® powder compacts lies in the interval 1000–1100 °C. The optimal sintering tempera-

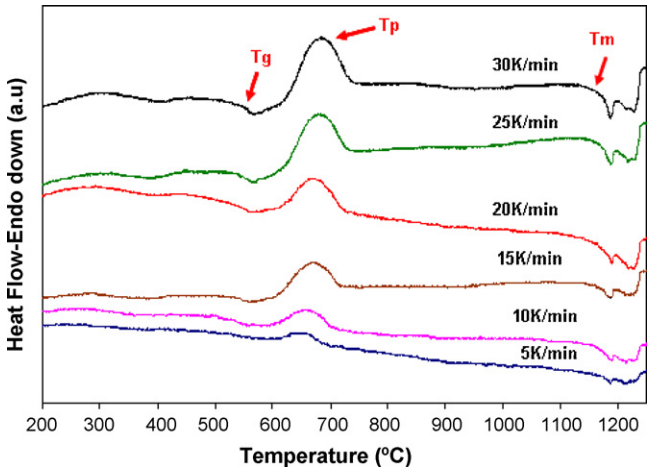

Fig. 7. DTA curves obtained for Bioglass® powder at different heating rates.

ture can be chosen in the centre of this interval, i.e. at 1050 °C, when viscous flow sintering dominates, as also indicated by the isothermal sintering study (Fig. 3).

3.3. DTA analysis and phase characterisation

DTA curves of the Bioglass® powder at different heating rates in the range 5–30 °C/min are shown in Fig. 7. All curves present a large exothermic peak, between 600 and 750 °C, and two small endothermic peaks, in the range 1150–1250 °C. After cooling to room temperature, all samples had a glassy aspect, indicating that at least partial melting has occurred during the DTA measurement. The large, broad exothermic peak mentioned above corresponds to Bioglass® crystallisation, while the two endothermic peaks represent melting processes, e.g. melting of two crystalline phases, as discussed in the literature.[13]

The characteristic temperatures (T_g, T_p and T_m) for the different heating rates are shown in Table 2. By increasing the heating rate, the glass transition temperature (T_g) and the peak crystallisation temperature (T_p) increase, while the onset melting temperature (T_m) decreases. These results are in agreement with those presented by Clupper and Hench.[20] For heating rates between 5 and 30 °C/min, the T_g varies in the range 500–550 °C. Bioglass® crystallises between 600 and 750 °C and starts to melt at temperature between 1150 and 1180 °C. During the crystallisation process the development of two crystalline phases is detected. The main crystalline phase is a sodium calcium silicate phase and the secondary one is a phosphate phase, which can be identified by FTIR. The FTIR spectra at the characteristic temperatures during and after heat treatment at temperatures in the range 600–800 °C are shown in Fig. 8, confirming the formation of the specific crystalline phases in this temperature range under the particular heat treatment used. The FTIR spectra of Bioglass® before heat treatment and of the sodium calcium silicate phase are also shown for comparison. The melting process of the two crystalline phases results in the occurrence of the two endothermic peaks at 1150–1180 °C. These findings are confirmed by previous work in the literature.[11,13,14] The FTIR spectra appear similar to those presented by Filho et al.[21] indicating a high degree of crystallinity under the specific heat treatment. The observation of the $Na_2Ca_2Si_3O_9$ phase was also confirmed by TEM in samples heat treated under the same conditions (Fig. 9), while the identification of the secondary phosphate phase was not possible. The $Na_2Ca_2Si_3O_9$ phase crystallised in hexagonal system and the characteristic lattice parameters are presented in Table 3. However, the presence of both crystalline phases was also confirmed by XRD analysis in samples heat treated up to 800 °C (Fig. 10). XRD analysis enabled the

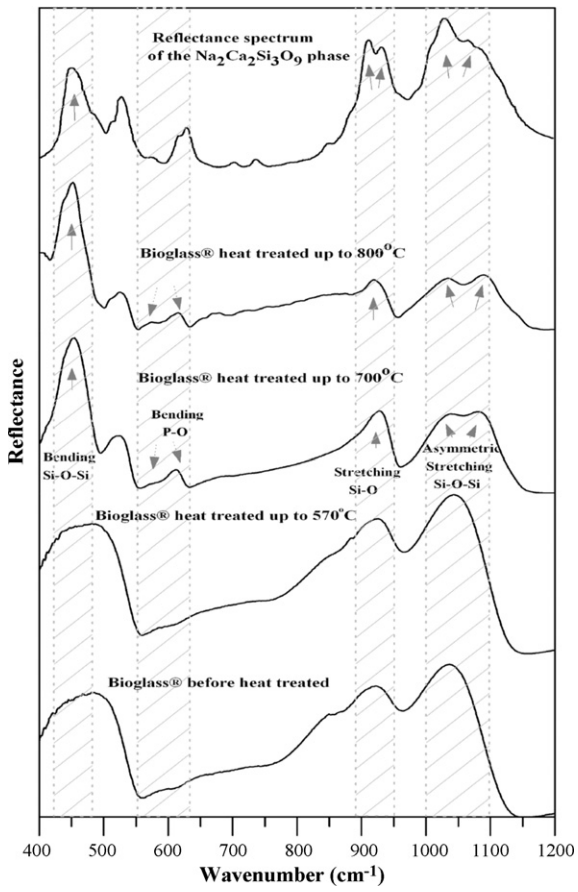

Fig. 8. FTIR spectra of Bioglass® before heat treatment, heat treated up to 570, 700 and 800 °C. Additionally, the characteristic spectra of the sodium calcium silicate ($Na_2Ca_2Si_3O_9$) phase is presented for comparison.

Table 2
DTA parameters at different heating rates.

Rate (°C/min)	T_g (°C)	T_p (°C)	T_m (°C)	*Hr*	*n*
5	505	650	1174	0.28	1.170
10	536	664	1172	0.25	0.964
15	544	674	1168	0.26	0.909
20	549	676	1165	0.26	0.886
25	553	686	1160	0.28	0.891
30	551	690	1155	0.30	0.886

Table 3
Characteristic lattice parameters of $Na_2Ca_2Si_3O_9$ crystal, hexagonal system.

a	*b*	*c*	*α*	*β*	*γ*
10.561	10.561	13.199	90°	90°	120°

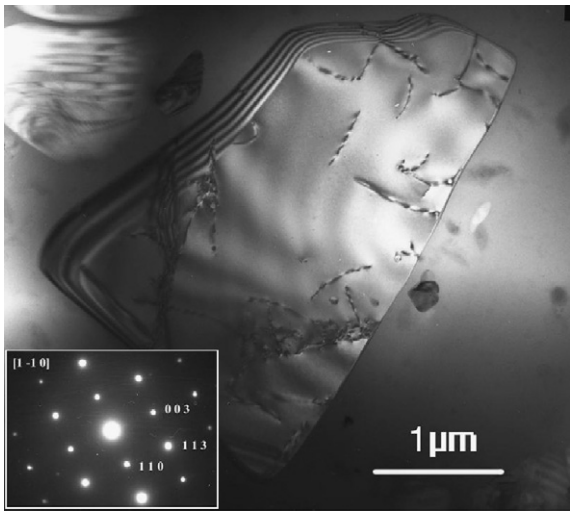

Fig. 9. TEM dark field image and electron diffraction pattern of the $Na_2Ca_2Si_3O_9$ phase formed during heat treatment of Bioglass® at temperatures higher than 600 °C.

precise identification of the secondary phosphate phase which was identified as silicorhenanite phase ($Na_2Ca_4(PO_4)_2SiO_4$), as expected also from the literature.[14]

The DTA characteristic temperatures are slightly different from data obtained by heating microscopy and dilatometry. These differences can be explained in terms of sample morphology. In the case of DTA, the samples were powders, while for the other techniques, the powder was compressed into powder compacts. In the last case, the compaction force reduces porosity between glass particles (green body density) and viscous flow sintering is facilitated. Therefore, the characteristic temperatures obtained using powder compacts are lower than those determined from DTA.

Considering the results from DTA, heating stage microscopy and dilatometry measurements, we can conclude that the first step of densification occurs shortly after the glass transition temperature is reached, when sintering takes place by viscous flow and particles are connected through sintering necks.[14] The Bioglass® particles crystallise in the range 600–750 °C, so the material is highly crystalline prior to undergoing the second stage of densification (above 850 °C). The shrinkage plateau observed between the two stages of sintering corresponds to the crystallisation process. During crystallisation, the viscosity increases and viscous flow sintering is inhibited.[17,22,23] With increasing temperature the viscosity decreases again, leading to the second sintering stage. Bioglass® powder compacts start the second stage of sintering above 850 °C. According to Lefebre et al.,[12,13] the second stage of sintering occurs after crystallisation of the secondary phosphate phase, in agreement with our results.

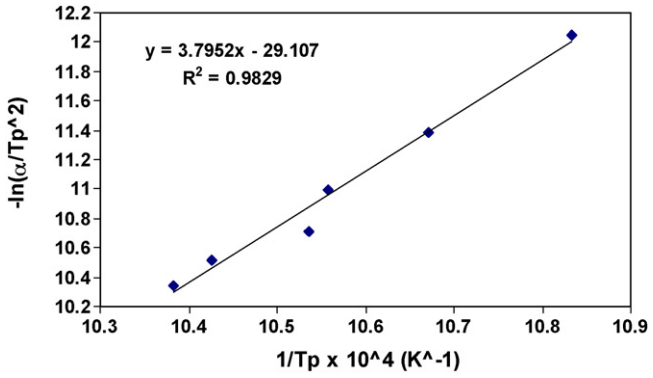

Fig. 11. Calculation of the activation energy for crystallisation from DTA results.

The plot of $[-\ln(\alpha/T_p^2)]$ versus $1/T_p$ is presented in Fig. 11. The correlation parameter ($R^2 = 0.9829$) indicates a very good fitting. The value of the activation energy for crystallisation calculated from the slope is 316 kJ/mol (Eq. (6)). This value is in agreement with the results obtained by other authors.[13,20] The values of the Avrami parameter n (Eq. (7)) for Bioglass® crystallisation at different heating rates are listed in Table 2. The average value is 0.95 ± 0.10 and thus a surface crystallisation is predominant in this material, as it was expected due to the very small particle size of the studied powder, which enhances the surface crystallisation mechanism.[23] The calculated values of the Hruby coefficient (Hr) (Eq. (8)) at different heating rates are shown in Table 2. The low mean value 0.27 ± 0.02 confirms a high crystallisation ability of Bioglass®, which has also been reported in the literature.[20]

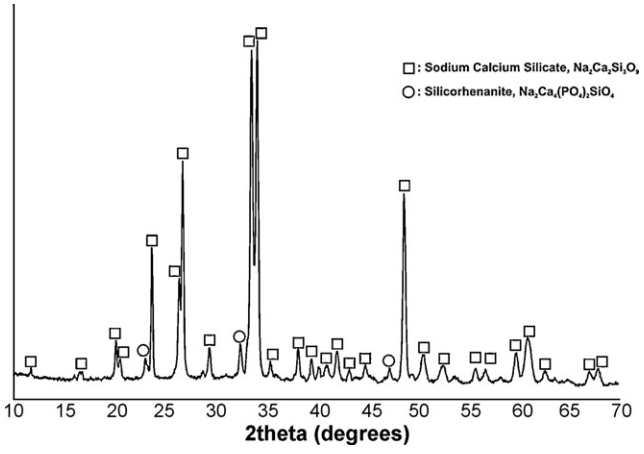

Fig. 10. XRD pattern of Bioglass® powder heat treated up to 800 °C, after the completion of the crystallisation process.

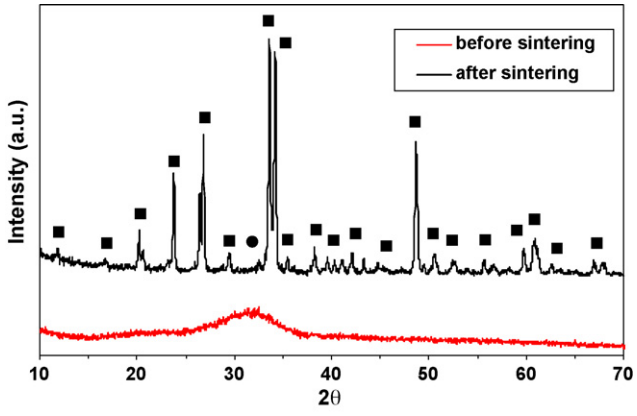

Fig. 12. XRD patterns of Bioglass® powder compacts before the heat treatment and after sintering at 1050 °C for 140 min (■ = $Na_2Ca_2Si_3O_9$, ● = $Na_2Ca_4(PO_4)_2SiO_4$).

The XRD patterns of Bioglass® powder compacts before heat treatment and after sintering at 1050 °C for 140 min are shown in Fig. 12. Before sintering, the XRD pattern of Bioglass® shows, as expected, that the material is completely amorphous but the sintered material exhibited a diffraction pattern characteristic of a glass–ceramic structure. The identified crystalline phases are the same to those observed on samples heat treated at temperatures after the completion of the crystallisation process (e.g. 800 °C) (Fig. 10). It is thus confirmed that the crystalline microstructure develops before the completion of sintering. The main crystalline phase is identified as $Na_2Ca_2Si_3O_9$, in agreement with our previous results on fabrication of scaffolds from the same Bioglass®.[6,14] The minor crystalline phase was also identified as $Na_2Ca_4(PO_4)_2SiO_4$ by Lefebre at al.[13]

4. Conclusions

The sintering process of 45S5 Bioglass® powder was studied by using different thermal analysis and microscopic methods. The Bioglass® powder sinters in two major steps: the first one in the temperature range 500–600 °C and the second one between 850 and 1100 °C. After sintering at 1050 °C for 140 min, considered to be the optimal isothermal sintering conditions, the main crystalline phase is $Na_2Ca_2Si_3O_9$ but other crystalline phases are possible under different heat treatment conditions, which are discussed in the literature[13]. It was confirmed that Bioglass® crystallises in the temperature range 600–750 °C, the exact crystallisation temperature depends on heating rate. Moreover, it was shown that Bioglass® powder has a high crystallisation ability and it crystallises by a surface crystallisation mechanism (Avrami parameter $n = 0.95$), so that the material is highly crystalline prior to undergoing the second step of densification (above 850 °C). Under the conditions of the experiments, which were carried out with equiaxed glass particles, there is no considerable shrinkage anisotropy during sintering. The results of the present investigation describing the interaction between crystallisation and viscous flow sintering in Bioglass® powder under different heat treatment conditions are relevant to support the fabrication of bone tissue engineering scaffolds from Bioglass®, which should exhibit tailored porosity, controlled crystallinity and enhanced bioactivity.

Acknowledgements

The authors acknowledge experimental assistance of Ms Tania Hoffer (RWTH Aachen) with the heating microscopy investigation and financial support from the EU via the Marie Curie fellowship scheme (Grant MEIF-CT-2005-024248).

References

1. Hench, L. L., Bioceramics. *J. Am. Ceram. Soc.*, 1998, **81**, 1705–1728.
2. Hench, L. L., Splinter, R. J., Allen, W. C. and Greenlee, T. K., Bonding mechanisms at the interface of ceramic prosthetic materials. *J. Biomed. Mater. Res.*, 1971, **2**, 117–141.
3. Hattar, S., Asselin, A., Greenspan, D., Oboeuf, M., Berdal, A. and Sautier, J. M., Potential of biomimetic surfaces to promote in vitro osteoblast-like cell differentiation. *Biomaterials*, 2005, **26**, 839–848.
4. Reilly, G. C., Radin, S., Chen, A. T. and Ducheyne, P., Differential alkaline phosphatase responses of rat and human bone marrow derived mesenchymal stem cells to 45S5 bioactive glass. *Biomaterials*, 2007, **28**, 4091–4097.
5. Xynos, I. D., Hukkanen, M. V., Batten, J. J., Buttery, L. D., Hench, L. L. and Polak, J. M., Bioglass 45S5 stimulates osteoblast turnover and enhances bone formation in vitro: implications and applications for bone tissue engineering. *Calcif. Tissue Int.*, 2000, **67**(4), 321–329.
6. Chen, Q. Z., Thompson, I. D. and Boccaccini, A. R., 45S5 Bioglass-derived glass–ceramic scaffolds for bone tissue engineering. *Biomaterials*, 2006, **27**, 2414–2425.
7. Peitl, O., LaTorre, G. P. and Hench, L. L., Effect of crystallization on apatite-layer formation of bioactive glass 45S5. *J. Biomed. Mater. Res.*, 1996, **30**(4), 509–514.
8. Clupper, D. C., Mecholsky, J. J., LaTorre, G. P. and Greenspan, D. C., Sintering temperature effects on the in vitro bioactive response of tape cast and sintered bioactive glass-ceramic in Tris buffer. *J. Biomed. Mater. Res.*, 2001, **57**(4), 532–540.
9. Rizkalla, A. S., Jones, D. W., Clarke, D. B. and Hall, G. C., Crystallisation of experimental bioactive glass compositions. *J. Biomed. Mater. Res.*, 1996, **32**, 119–124.
10. Peitl, O., Zanotto, E. D. and Hench, L. L., Highly bioactive P_2O_5–Na_2O–CaO–SiO_2 glass–ceramics. *J. Non-Cryst. Solids*, 2001, **292**(1–3), 115–126.
11. Chatzistavrou, X., Zorba, T., Kontonasaki, E., Chrissafis, K., Koidis, P. and Paraskevopoulos, K. M., Following bioactive glass behaviour beyond melting temperature by thermal and optical methods. *Phys. Stat. Sol. (a)*, 2004, **201**, 944–951.
12. Lefebvre, L., Gremillard, L., Chevalier, J., Zenati, R. and Bernache-Assolant, D., Sintering behaviour of 45S5 bioactive glass. *Acta Biomater.*, 2008, **4**, 1894–1903.
13. Lefebvre, L., Chevalier, J., Gremillard, L., Zenati, R., Thollet, G., Bernache-Assolant, D. and Govin, A., Structural transformations of bioactive glass 45S5 with thermal treatments. *Acta Mater.*, 2007, **55**, 3305–3313.
14. Boccaccini, A. R., Chen, Q. Z., Lefebvre, L., Gremillard, L. and Chevalier, J., Sintering, crystallisation and biodegradation behaviour of Bioglass®-derived glass–ceramics. *Faraday Discuss.*, 2007, **136**, 27–44.
15. Huang, R., Pan, J., Boccaccini, A. R. and Chen, Q. Z., A two-scale model for simultaneous sintering and crystallization of glass–ceramic scaffolds for tissue engineering. *Acta Biomater.*, 2008, **4**, 1095–1103.
16. Boccaccini, A. R. and Hamann, B., In-situ high temperature optical microscopy. A review. *J. Mater. Sci.*, 1999, **34**, 5419–5436.
17. Boccaccini, A. R., Stumpfe, W., Taplin, D. M. R. and Ponton, C. B., Densification crystallization of glass powder compacts during constant heating rate sintering. *Mater. Sci. Eng.*, 1996, **A219**, 26–31.
18. Liu, Y., Xiang, Q., Tan, Y. and Sheng, X., Nucleation and growth of needle-like fluorapatite crystals in bioactive glass–ceramics. *J. Non-Cryst. Solids*, 2008, **354**, 938–944.
19. Guo, X., Yang, H., Han, C. and Song, F., Crystallization and microstructure of Li_2O–Al_2O_3–SiO_2 glass containing complex nucleating agent. *Thermochim. Acta*, 2006, **444**, 201–205.
20. Clupper, D. C. and Hench, L. L., Crystallization kinetics of tape cast bioactive glass 45S5. *J. Non-Cryst. Solids*, 2003, **318**, 43–48.
21. Filho, P. O., LaTorre, P. G. and Hench, L. L., Effect of crystallization on apatite-layer formation of bioactive glass 45S5. *J. Biomed. Mater. Res.*, 1996, **30**, 509–514.
22. Prado, M. O., Fredericci, C. and Zanotto, E. D., Non-isothermal sintering with concurrent crystallization of polydispersed soda–lime–silica glass beads. *J. Non-Cryst. Solids*, 2003, **331**, 157–167.
23. Chatzistavrou, X., Zorba, T., Chrissafis, K., Kaimakamis, G., Kontonasaki, E., Koidis, P. and Paraskevopoulos, K. M., Influence of particle size on the crystallization process and the bioactive behavior of a bioactive glass system. *J. Therm. Anal. Calorimet.*, 2006, **85**, 253–260.